AGU PUBLICATIONS

JGR

Journal of Geophysical Research: Atmospheres

RESEARCH ARTICLE
10.1002/2014JD022221

Key Points:
- This is the first study to document the robust impact of the VM on ENSO
- The findings may have profound implications for ENSO prediction
- This study provides further evidence of the extratropical influence on ENSO

Correspondence to:
J. Li,
ljp@bnu.edu.cn

Citation:
Ding, R., J. Li, Y.-h. Tseng, C. Sun, and Y. Guo (2015), The Victoria mode in the North Pacific linking extratropical sea level pressure variations to ENSO, *J. Geophys. Res. Atmos.*, *120*, 27–45, doi:10.1002/2014JD022221.

Received 24 JUN 2014
Accepted 2 DEC 2014
Accepted article online 5 DEC 2014
Published online 8 JAN 2015

The Victoria mode in the North Pacific linking extratropical sea level pressure variations to ENSO

Ruiqiang Ding[1], Jianping Li[2], Yu-heng Tseng[3], Cheng Sun[2], and Yipeng Guo[1]

[1]State Key Laboratory of Numerical Modeling for Atmospheric Sciences and Geophysical Fluid Dynamics, Institute of Atmospheric Physics, Chinese Academy of Sciences, Beijing, China, [2]College of Global Change and Earth System Sciences, Beijing Normal University, Beijing, China, [3]Climate and Global Dynamics Division, NCAR, Boulder, Colorado, USA

Abstract The Victoria mode (VM) represents the second dominant mode (empirical orthogonal function, EOF2) of North Pacific variability, independent of the Pacific Decadal Oscillation and is defined as the EOF2 of SST anomalies in the North Pacific poleward of 20°N. The present study indicates that the VM is closely linked to the development of El Niño–Southern Oscillation (ENSO). The VM may effectively act as an ocean bridge (or conduit) through which the extratropical atmospheric variability in the North Pacific influences ENSO. The VM can trigger the onset of ENSO via the following two dominant processes: (1) surface air-sea coupling associated with the VM in the subtropical/tropical Pacific and (2) evolution of subsurface ocean temperature anomalies along the equator associated with the VM. These two processes may force sufficient surface warming to occur in the central eastern equatorial Pacific from spring to summer, which in turn initiates an ENSO event. The VM influence on ENSO relies on a basin-scale air-sea interaction dynamic, as opposed to more local-scale dynamics typically associated with the seasonal footprinting mechanism or Pacific meridional mode. The majority of VM events are followed by ENSO events. These ENSO events triggered by VM include El Niño Modoki (EM) as well as conventional El Niño. There is no evidence that the VM tends to be more conducive to the initialization of EM than conventional El Niño.

1. Introduction

The Pacific Decadal Oscillation (PDO) is defined as the leading empirical orthogonal function (EOF) of monthly sea surface temperature (SST) anomalies (SSTAs) in the North Pacific poleward of 20°N [*Mantua et al.*, 1997; *Zhang et al.*, 1997]. The spatial pattern of the PDO resembles a horseshoe, with SST anomalies of one sign in the central North Pacific surrounded by anomalies of opposite sign in the Gulf of Alaska, off California, and toward the tropics. The PDO exhibits pronounced "phase shifts" at 20 to 30 year intervals, with the 1976–1977 shift being the most well known and extensively studied [e.g., *Nitta and Yamada*, 1989; *Graham*, 1994; *Miller et al.*, 1994; *Trenberth and Hurrell*, 1994; *Hare and Mantua*, 2000; *Deser and Phillips*, 2006].

Previous studies have documented the wide-ranging impacts of the PDO on Northern Hemisphere climate (e.g., North American precipitation, stream flow, and surface temperature anomalies) and on the North Pacific ecosystem [*Mantua et al.*, 1997; *Zhang et al.*, 1997; *Mantua and Hare*, 2002]. However, as noted by *Bond et al.* [2003] and *Di Lorenzo et al.* [2008], the PDO alone does not fully characterize the North Pacific climate. Their analysis demonstrated that additional modes may significantly influence the climatic variability of the North Pacific. Using EOF analysis, they introduced a mode known as the Victoria mode (VM) [*Bond et al.*, 2003] or North Pacific Gyre Oscillation (NPGO) [*Di Lorenzo et al.*, 2008] to describe aspects of low-frequency variability that cannot be explained by the PDO alone. The VM is defined as the second dominant mode (EOF2) of SSTAs in the Pacific north of 20°N, while the NPGO is defined as the EOF2 of SSH (sea surface height) anomalies (SSHAs) in the central and eastern North Pacific (180°W–110°W, 25°N–62°N). Both modes are forced by the atmosphere through the North Pacific Oscillation (NPO) [*Walker and Bliss*, 1932; *Rogers*, 1981] and are distinct from the PDO, which is linked to variations of the Aleutian Low [*Bond et al.*, 2003; *Di Lorenzo et al.*, 2008]. The NPGO index (the second principal component (PC2) of SSHA; NPGO index (NPGOI)) measures changes in the North Pacific gyre circulation, including the North Pacific Current and the Kuroshio-Oyashio Extension [*Di Lorenzo et al.*, 2008; *Ceballos et al.*, 2009]. The NPGO is also

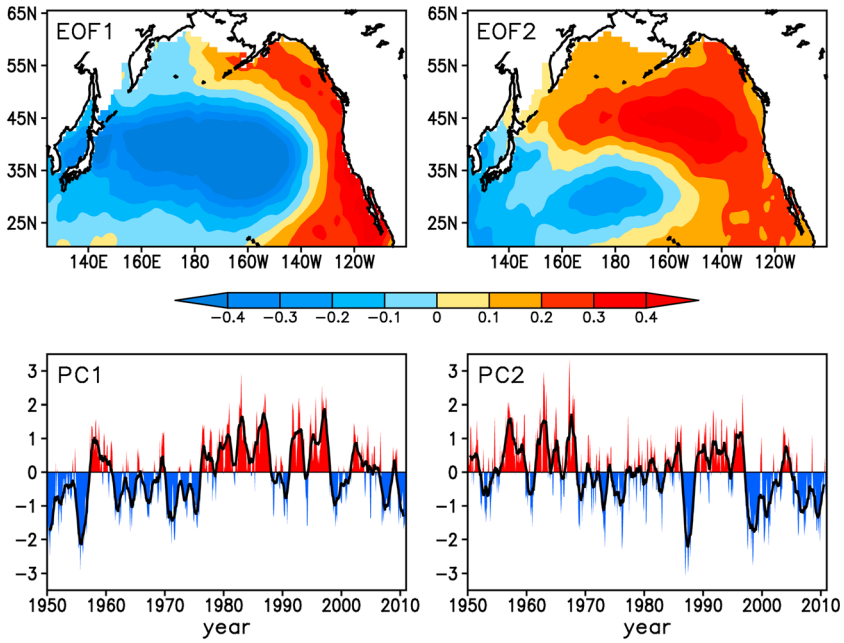

Figure 1. Spatial patterns and corresponding PCs of the first two leading EOF modes of the North Pacific (124.5°E–100.5°W, 20.5°N–65.5°N) monthly SSTA field (after removing the monthly mean global average SSTA). Monthly values of PC1 and PC2 time series are indicated by colored bars (red, positive and blue, negative) with a 13 month running mean overlain (bold lines).

significantly correlated with decadal variations of salinity and key biological parameters including chlorophyll *a* and NO_3 throughout the Northeast Pacific [*Di Lorenzo et al.*, 2008, 2009a] and Japanese eel recruitment in the western Pacific [*Tzeng et al.*, 2012]. In contrast, few studies have examined the effect of the VM on climate and ecosystems, as both the NPGO and VM are considered to represent the second mode of the North Pacific variability and to therefore have similar impacts on climate and ecosystems.

However, the SSH and SST variations are not completely consistent, as the SSH variations are influenced by ocean circulation and salinity as well as ocean temperature. There are in fact remarkable differences between the VM and NPGO indices. *Di Lorenzo et al.* [2008] found that the NPGOI closely tracks the VM index (PC2 of SSTA in the Pacific north of 20°N; VMI), with a correlation coefficient (*R*) of 0.55, but the NPGOI exhibits more prominent low-frequency (decadal) fluctuations than the VMI, reflecting the different damping time scales operating on the SST and SSH.

Following *Bond et al.* [2003], we performed EOF analysis of the monthly SSTA field over the North Pacific (124.5°E–100.5°W, 20.5°N–65.5°N) for the period 1950–2011 (after removing the monthly mean global average SSTA) (Figure 1). The structure of EOF1, which accounts for 25.7% of the total variance, closely resembles the PDO pattern [*Mantua et al.*, 1997; *Zhang et al.*, 1997]. The PC1 exhibits considerable variability on decadal scales, including a notable climate shift around 1976–1977. This mode is herein referred to as the PDO. The EOF2, which accounts for 12.4% of the total variance, exhibits a distinct northeast-southwest oriented dipole pattern, with a band of positive SSTA extending from off California across the Pacific to the western Bering Sea, and a band of negative SSTA extending from the central North Pacific to the coast of Asia, which closely resembles the spatial pattern of the VM of *Bond et al.* [2003]. Hereafter, we refer to this SST EOF2 mode as the so-called VM.

The power spectra of the NPGOI (available online at http://www.o3d.org/npgo/data/NPGO.txt) and VMI (the normalized PC2 time series associated with the EOF2 in Figure 1) are shown in Figures 2a and 2b, respectively. The NPGO exhibits a significant (at the 90% level) spectral peak around 10 years that is absent from the VM; instead, the VM tends to have higher power at interannual time scales, with a peak at periods of 3–4 years (but not significant at the 90% level). The damping time scale of the VM was computed from its decorrelation time scale as about 4 months. According to *Di Lorenzo et al.* [2010] and

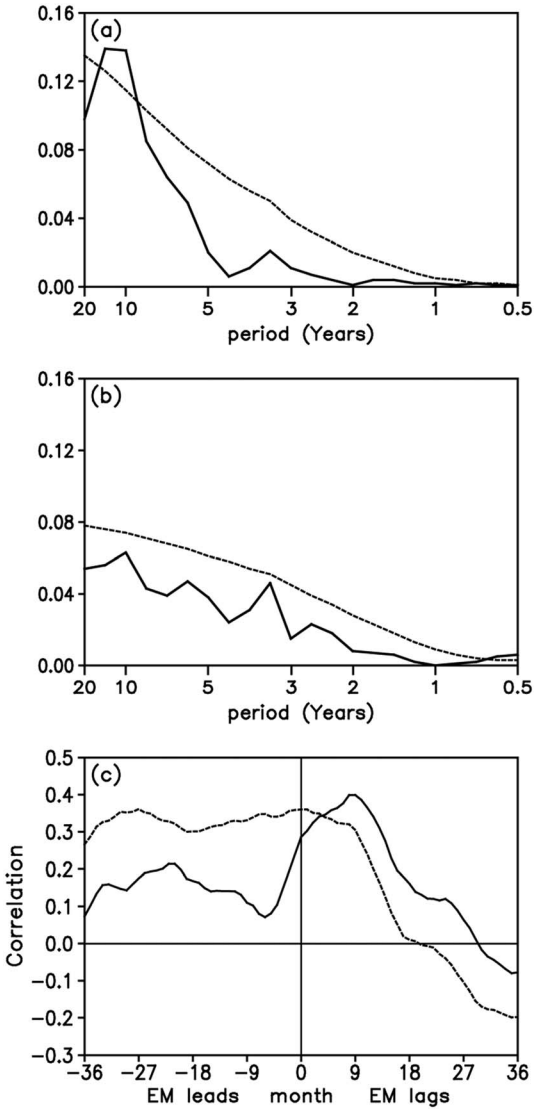

Figure 2. Power spectra of the raw monthly (a) NPGOI and (b) VMI for the period 1950–2011. The dashed lines represent the 90% significance level for a red noise spectrum. (c) Lead-lag correlations of the raw monthly electromagnetic interference with the raw monthly VM (solid line) and NPGO (dashed line) indices.

Chhak et al. [2009], the damping time scale of the NPGO is about 10 months, which is about twice that of the VM, suggesting that the NPGO has greater low-frequency power than the VM, consistent with the spectra of NPGO and VM indices.

Furthermore, recent studies have reported two different types of El Niño event, which may result from different dynamical processes and responses. *Ashok et al.* [2007] referred to the new type of El Niño as El Niño Modoki (EM). Also, named as the Date Line El Niño [*Larkin and Harrison*, 2005], warm-pool El Niño [*Kug et al.*, 2009], or the Central Pacific warming El Niño [*Kao and Yu*, 2009; *Yeh et al.*, 2009], EM exhibits maximum positive SSTAs in the central tropical Pacific, rather than the eastern tropical Pacific as seen during conventional ENSO episodes. Some recent studies have linked EM variability with NPGO variability [*Di Lorenzo et al.*, 2010; *Furtado et al.*, 2012], showing that atmospheric teleconnections generated by EM influence the NPO (mainly the southern pole of the NPO), and are then low pass filtered by the ocean, leading to the decadal-scale NPGO variability. This revealed an important link among EM, NPO, and NPGO on decadal time scales as follows: EM → NPO → NPGO, where the arrows show the cause-and-effect relationships. Lead-lag correlations between the NPGOI and EM index (EMI; available online at www.jamstec.go.jp/frsgc/research/d1/iod/DATA/emi.monthly.txt) indicate that strong positive correlations indeed occur when EM leads the NPGO by a few months to almost 3 years (Figure 2c). Note that positive correlations also occur when the NPGO leads EM by a few months to more than a year. However, in comparison, for lead times of a few months to more than a year, the VM shows stronger correlations than the NPGO with EM. These results suggest that the VM and NPGO seem to have a different dynamical linkage with ENSO variability in the tropical Pacific. Although NPGO → ENSO has been presented in the literature [*Di Lorenzo et al.*, 2009b], VM → ENSO should also require a thorough investigation because the enhanced power on interannual time scales shown in the VM power spectrum could potentially be more important for ENSO.

Previous studies have suggested a physical connection between extratropical atmospheric variability over the North Pacific in a particular winter and ENSO in the following winter [*Vimont et al.,* 2001, 2003a, 2003b; *Anderson*, 2003; *Alexander et al.*, 2010; *Yu and Kim*, 2011]. The mechanisms responsible for the link between extratropical atmospheric variability and ENSO have been extensively studied. There are at least three mechanisms through which extratropical atmospheric variability may influence ENSO: (1) the SST "footprint" induced by the wintertime NPO persists until late spring and summer when its subtropical portion (0°–20°N) forces the overlying atmosphere, resulting in zonal wind stress anomalies that favor the initiation of an ENSO event (the seasonal footprinting mechanism (SFM)) [*Vimont et al.,* 2001, 2003a, 2003b]; (2) an anomalous

north-south SSTA gradient in the tropical eastern Pacific coupled with anomalous southwesterlies in the northeasterly trade regime force energetic equatorially trapped oceanic waves to occur in the central western Pacific through the thermodynamic air-sea coupling, which in turn initiate an ENSO event (the Pacific meridional mode (PMM) mechanism) [*Chiang and Vimont*, 2004; *Chang et al.*, 2007; *Zhang et al.*, 2009a]; and (3) the NPO-induced variations in the North Pacific trade winds can directly force subsurface temperature anomalies across the central equatorial Pacific that are conducive to initiating an ENSO event (the trade wind charging mechanism (TWC)) [*Anderson*, 2004; *Anderson et al.*, 2013a].

In the present paper, we show that the VM, an independent mode of North Pacific SST variability with respect to the PDO, may act as an effective link between extratropical atmospheric variability and ENSO variability. The cause-and-effect relationships among the NPO, VM, and ENSO, which are robust on monthly to seasonal time scales, are as follows: NPO → VM → ENSO. The strong relationship between the VM and ENSO may have profound implications for ENSO prediction. In addition to establishing the link between the VM and ENSO, we further explore questions regarding the influences of the VM on ENSO, such as why some VM events can excite ENSO while some cannot and whether the VM tends to be more conducive to the initialization of EM than conventional El Niño.

The remainder of this paper is organized as follows. Section 2 describes the observed data, method, and numerical model used in this study. Section 3 establishes the atmospheric forcing of the VM by the NPO and quantifies the fraction of VM variability driven by the NPO. Section 4 explores the link between the VM and ENSO, and the mechanism by which the VM forces the onset of ENSO events. Finally, section 5 summarizes and discusses the major results.

2. Data, Method, and Model

2.1. Observational Data

The SST data set used in this study is the Hadley Centre global sea ice and sea surface temperature (HadISST) data on a 1° × 1° grid [*Rayner et al.*, 2006]. For subsurface ocean temperature information, we used the Simple Ocean Data Assimilation (SODA) version 2.2.4 for the period 1950–2008 [*Carton and Giese*, 2008]. The SODA data set has 40 vertical levels unevenly distributed from 5 to 5375 m and covers the global oceans from 75.25°S to 89.25°N with a horizontal resolution of 0.5° × 0.5°. For the atmospheric fields, we use the National Centers for Environmental Prediction-National Center for Atmospheric Research (NCEP-NCAR) reanalysis on a 2.5° × 2.5° grid [*Kalnay et al.*, 1996]. The NCEP-NCAR reanalysis used in this study includes spherical Langmuir probe (SLP) and surface wind fields for the period 1950–2011. In this paper, the monthly anomalies are computed by removing the climatological monthly means.

2.2. Effective Number of Degrees of Freedom

We estimate the significance of all correlations between two time series taking into account the effect of their autocorrelations, which reduces the effective number of degrees of freedom. For the correlation between monthly data of variables x and y, the effective sample size N^* is computed by considering the lag–1 autocorrelations of variable x and variable y following *Bretherton et al.* [1999]:

$$N^* = N\frac{1 - r_x r_y}{1 + r_x r_y},$$

where N is the number of available time steps and r_x and r_y are the lag 1 autocorrelations of variables x and y, respectively.

2.3. Numerical Model

The numerical experiments presented in this paper are based on the Community Atmosphere Model version 5.0 (CAM5) [*Neale et al.*, 2010]. CAM5 is the atmospheric component of the Community Earth System Model developed primarily at the National Center for Atmospheric Research (NCAR) and is the latest version of the CAM and contains a range of significant enhancements and improvements in the representation of physical processes over its previous versions including CAM3 and CAM4. CAM5 has 30 vertical levels extending from the ground to 2.25 hPa with a horizontal resolution of 1.9° × 2.5° in latitude and longitude.

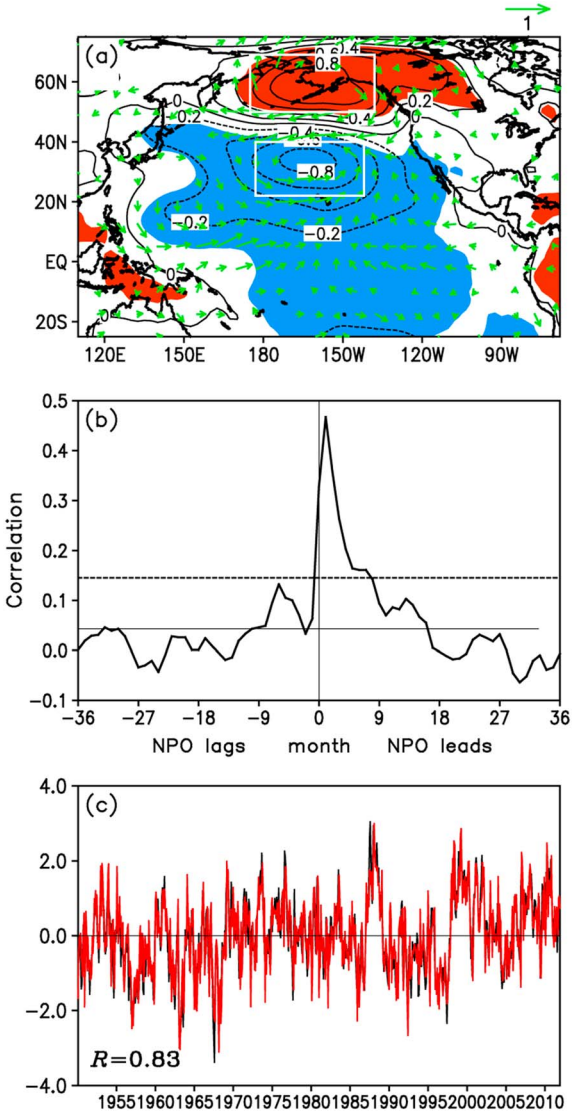

Figure 3. (a) Pacific SLP (mbar; contours) and surface wind (m s^{-1}; vectors) anomalies regressed on the VMI. The two white boxes denote the locations of the northern (175°E–138°W, 50°N–69°N) and southern (177°E–142°W, 22°N–40°N) poles of the NPO, respectively; the difference between the normalized SLP anomalies averaged over each pole is used to define the NPOI. Positive (red) and negative (blue) SLP anomalies, with regression coefficients significant at the 95% level, are shaded; only surface wind vectors significant at the 95% level are shown. (b) Lead-lag correlation coefficients between the raw monthly VM and NPO indices; the horizontal dashed line indicates the 99.9% significance level. (c) Observed VMI (black line) and reconstructed VMI (red line) using an AR1 model forced by the NPOI. The correlation coefficient (*R*) between the monthly values of observed and reconstructed VM indices is 0.83, significant at the 99.9% level.

3. Atmospheric Forcing of the VM

Previous studies have linked the atmospheric forcing of the NPGO to the NPO, and quantified the fraction of NPGO variability driven by the NPO [*Chhak et al.*, 2009]. In addition, they have analyzed in detail how NPO-like atmospheric variability induces changes in surface heat fluxes that in turn generate SSTAs in the North Pacific [*Vimont et al.,* 2003a, 2003b; *Alexander et al.*, 2010; *Yu and Kim*, 2011]. However, the fraction of the VM variability driven by the NPO, considered as an independent mode of North Pacific SST variability with respect to the PDO, remains unknown. Considering the differences between the VM and NPGO, it is necessary to examine further the contribution of NPO forcing to VM variability.

We first identify the SLP and surface wind anomalies associated with the VM by regressing Pacific SLP and surface wind anomalies onto the VMI. As shown in Figure 3a, the SLP pattern associated with the VM exhibits a meridional dipole structure, characterized by out-of-phase SLP variations over the northern and southern poles with a nodal point near 45°N. This pattern resembles the NPO [*Walker and Bliss*, 1932; *Rogers*, 1981]. This SLP dipole pattern associated with the VM is herein referred to as the NPO. The NPO index (NPOI) is defined as the difference between the normalized SLP anomalies averaged over the northern (175°E–138°W, 50°N–69°N) and southern (177°E–142°W, 22°N–40°N) poles (Figure 3a). The SLP anomalies associated with the VM are consistent with surface wind anomalies.

We calculate the lead-lag correlations between the VM and NPO indices (Figure 3b). The strongest correlation ($R = 0.47$; significant at the 99.9% level) occurs when the NPO leads the VM by 1 month, indicating a significant influence of the atmosphere on the ocean. As reported by *Alexander et al.* [2010] and *Yu and Kim* [2011], anomalous surface wind associated with the NPO can force a tripole-like pattern of the surface heat flux anomalies in the North Pacific, which in turn induces a tripole SSTA pattern there (including a dipole SSTA pattern of the VM in the North Pacific poleward of 20°N, along with a subtropical pole of positive SSTAs located in the central eastern North Pacific).

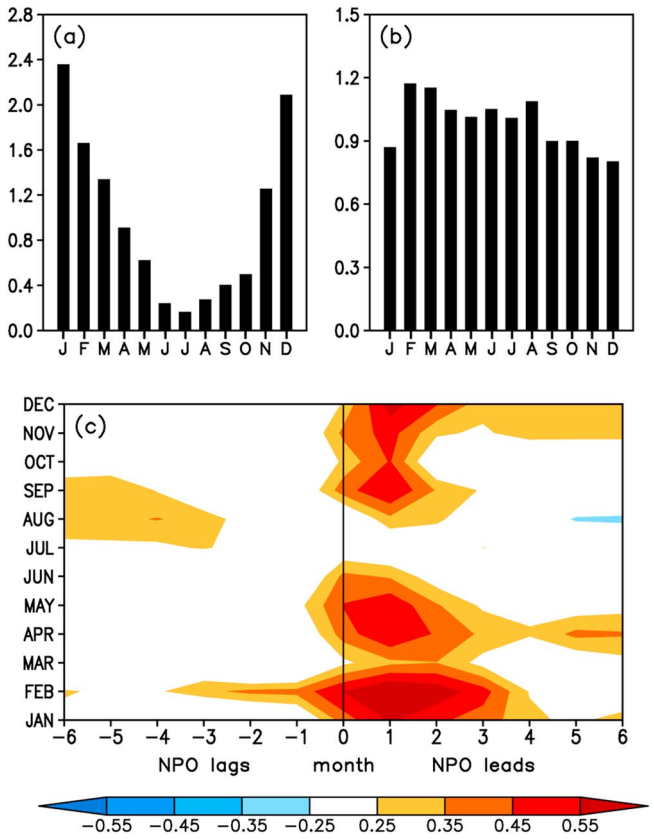

Figure 4. (a) Seasonal variations of the standard deviation of the NPOI. (b) Seasonal variations of the standard deviation of the VMI. (c) Seasonal dependence of lead-lag correlations between the monthly VM and NPO indices. Areas with the correlation coefficients significant at the 95% level are shaded.

To quantify the oceanic response of the VM to the atmospheric forcing of the NPO, we follow the approach of *Newman et al.* [2003] and *Schneider and Cornuelle* [2005] and assume that the change of the monthly VM is governed by an autoregressive model of order 1 (AR1),

$$\mathrm{VM}_{t+1} = \alpha \cdot \mathrm{NPO}_t + \beta \cdot \mathrm{VM}_t + \eta_t, \quad (1)$$

where the first and second terms on the right-hand side represent the NPO forcing index and the damping term, respectively, and η_t is uncorrelated noise. The coefficients $\alpha = 0.47$ and $\beta = 0.68$ are obtained from observations by regressing the VM against the previous month's NPO, removing the NPO term, then regressing the residual against the previous month's VM. The reconstructed monthly VMI obtained from equation (1) and the raw monthly VMI show almost the same variability; both have a strong correlation ($R = 0.83$, significant at the 99.9% level) (Figure 3c). This suggests that the NPO may account for a large fraction ($> 60\%$) of the VM variability.

Figures 4a and 4b show the seasonal variations in the standard deviations of the NPO and VM indices. We can see that the NPO attains maximum variance in winter (December–February (DJF)), while the VM shows a large variance in late winter and early spring (February–April (FMA)). It is very likely that the strong VM during FMA is a delayed (by about 1–2 months) response to the forcing of the DJF NPO. In addition, we note that the variance of the VM shows a small change from February to August, and the VM still shows a relatively marked variance in summer (June–August (JJA)). As shown in Figure 4c, for lead times of 1–2 months, the NPO has strong correlations with the VM throughout the year, except during summer months (JJA) when the NPO is weakest. The results suggest that the influence of the NPO on the VM is relatively weak in summer, while this influence is mainly confined to the other three seasons. The marked variance of the summer VM may be mainly due to the influence of the seasonal variation of the ocean mixed layer depth (MLD) in the extratropical North Pacific. The MLD in the extratropical North Pacific is observed to be deep in winter and shallow in summer, consistent with the seasonal variation of surface wind stress [*Deser et al.*, 2003; *Ding and Li*, 2009]. The shallow MLD in the extratropical North Pacific tends to amplify the VM-related SST response to atmospheric surface wind anomalies and therefore tends to cause a relatively marked variance of the VM in summer. These results indicate that the response of the VM to the atmospheric forcing of the NPO is possibly modulated by the seasonal variations of the MLD. Further study is required to perform a quantitative analysis of the relative contributions of the NPO and MLD on the seasonality of the VM variability.

4. Establishing the VM-ENSO Relationship

4.1. Lead-Lag Relationships Between the VM and ENSO

Section 3 established that the VM is a direct oceanic response to the atmospheric forcing of the NPO. We now turn to the relationships between the VM and ENSO which were not addressed previously. Considering that

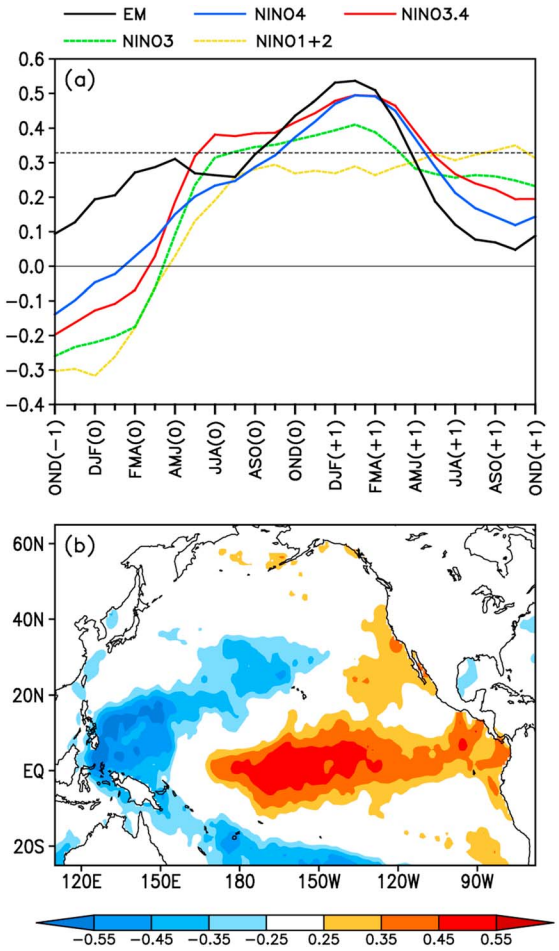

Figure 5. (a) Lead-lag correlations between the FMA(0)-averaged VMI and overlapping 3 month averaged values of Niño1 + 2 (90°W–80°W, 10°S–0°), Niño3 (150°W–90°W, 5°S–5°N), Niño3.4 (170°W–120°W, 5°S–5°N), Niño4 (160°E–150°W, 5°S–5°N), and EM indices (–1: year prior to the VMI; 0: year concurrent with the VMI; and +1: year followed by the VMI). The horizontal dashed line shows the 99% significance level. (b) Correlation maps of the FMA(0)-averaged VMI with the following JFM(+1) SSTAs. Areas with correlation significant at the 95% level are shaded.

the NPO peaks in winter and the SST footprint forced by the NPO (i.e., the VM) is strongest in late winter and early spring (FMA), we compute lead-lag correlations between the FMA-averaged VMI and 3 month averaged ENSO indices (including the Niño1 + 2, Niño3, Niño3.4, and Niño4 indices) (Figure 5a). Hereafter, we denote the year in which the VM peaks in FMA as year 0 and the preceding and following years as year –1 and +1, respectively. For the Niño3, Niño3.4, and Niño4 indices, their peak correlations (all significant at the 99% level) occur during JFM(+1), lagging the peak of the VM during FMA (0) by about 11 months. In comparison, the peak correlations between the VM and Niño3.4 indices, and between the VM and Niño4 indices, are very close, both of which are higher than that between the VM and Niño3 indices. For lead times of a few months to more than a year, the VMI shows much weaker (not significant at the 99% level) correlations with the Niño1 + 2 index than those with other ENSO indices (including the Niño3, Niño3.4, and Niño4 indices).

Correlation maps of the FMA(0) VMI with the following JFM(+1) SSTAs indicate that the warming center related to the VM is located in the central tropical Pacific (between 180° and 130°W), covering the eastern part of the Niño4 region (160°E–150°W, 5°S–5°N) and almost the entire Niño3.4 region (170°W–120°W, 5°S–5°N) (Figure 5b). In contrast, there is relatively weak warming related to the VM in the eastern tropical Pacific, especially in the Niño1 + 2 region (90°W–80°W, 10°S–0°), consistent with the results shown in Figure 5a.

Furthermore, we apply a maximum covariance analysis (MCA; also known as singular value decomposition) [*Bretherton et al.*, 1992] to the cross-covariance matrix between the FMA(0) North Pacific (124.5°E–100.5°W, 20.5°N–65.5°N) SSTAs and the following JFM(+1) tropical Pacific (124.5°E–100.5°W, 20.5°S–20.5°N) SSTAs. The leading MCA mode explains 69% of the total squared covariance. The correlation coefficient between the corresponding expansion coefficients is 0.63 (Figure 6c), which is significant at the 99.9% level. The expansion coefficients of the FMA(0) North Pacific and JFM(+1) tropical Pacific SSTAs have strong correlations of 0.98 and 0.95, respectively, with the FMA(0) VMI and JFM(+1) Niño3.4 index. This indicates that two MCA time series may be used to represent the VM and ENSO variability, respectively.

Figures 6a and 6b show the leading pair of heterogeneous patterns, which are generated by correlating the respective heterogeneous SSTA field with the MCA leading normalized expansion coefficients. The FMA(0) North Pacific is dominated by a tripole SSTA pattern (including a dipole SSTA pattern of the VM in the North Pacific poleward of 20°N, along with a subtropical pole of positive SSTA located in the central eastern North Pacific). During the following winter, the tropical Pacific SSTA pattern bears a strong resemblance to the correlation map in Figure 5b, with maximum warming in the central tropical

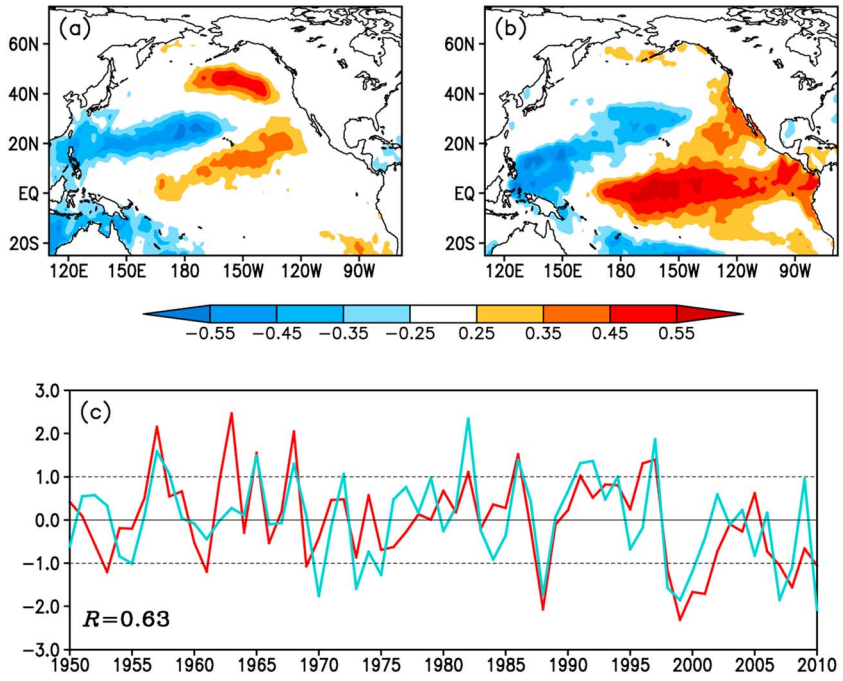

Figure 6. Spatial properties of the leading MCA mode for (a) the FMA(0) North Pacific (124.5°E–100.5°W, 20.5°N–65.5°N) SSTA field and (b) the following JFM(+1) tropical Pacific (124.5°E–100.5°W, 20.5°S–20.5°N) SSTA field, shown as correlation maps of the respective heterogeneous SSTA field with the MCA leading normalized expansion coefficients. (c) The MCA leading normalized expansion coefficients of the FMA(0) North Pacific SSTA filed (red line) and the following JFM(+1) tropical Pacific SSTA field (light blue line). In Figures 6a and 6b, areas with correlation significant at the 95% level are shaded. In Figure 6c, the correlation between two time series is given in the lower left corner, and the horizontal dashed lines indicate ± one standard deviation.

Pacific, almost symmetrical about the equator. These patterns suggest that a strong VM event in later winter and early spring tends to be followed by a strong ENSO event during the following winter. This result agrees with the conclusions from Figures 5a and 5b and confirms the strong connection between the FMA(0) VM and JFM(+1) ENSO. The VM SST pattern bears a resemblance to the optimal initial SST condition that is the most likely to develop into a strong ENSO event [*Penland and Sardeshmukh*, 1995]. *Anderson* [2003] performed a similar MCA analysis but using SLP as the leading field, which also resulted in the identification of much the similar precursor SST pattern (obtained by regressing the SSTA field onto the preceding SLP index) as presented here.

In addition, it is important to point out that the relationship between the VM and ENSO seems to be much more robust than the direct relationship between the NPO and ENSO. This conclusion is supported by the fact that the VM has stronger and more significant correlations with various ENSO indices than does the NPO for lead times of a few months to more than a year (not shown). The peak correlation (0.37) between the FMA(0) NPO and JFM(+1) Niño3.4 indices is lower than that (0.49) between the FMA(0) VM and JFM(+1) Niño3.4 indices. This result might be expected, considering that an index based on atmospheric variables like the NPO is likely much noisier than the one based on oceanic variables like the VM. This finding is consistent with the idea that the NPO may provide an important source of atmospheric forcing to excite the VM (i.e., the SST footprint) [*Vimont et al.,* 2001, 2003a, 2003b]; however, the VM, as an ocean bridge (or conduit) linking the NPO to ENSO, is more directly linked to ENSO than the atmospheric forcing itself. Nevertheless, it should be noted that, although the NPO by its original definition denotes a seesaw structure of SLP between Alaska and Hawaii, its individual poles may play different roles in Pacific climate variability [*Furtado et al.*, 2012]. The southern pole of the NPO—which represents a separate but related center of action with regard to its northern counterpart [*Furtado et al.*, 2012]—most likely results in more substantial correlations with ENSO than the full NPO index [*Anderson*, 2003].

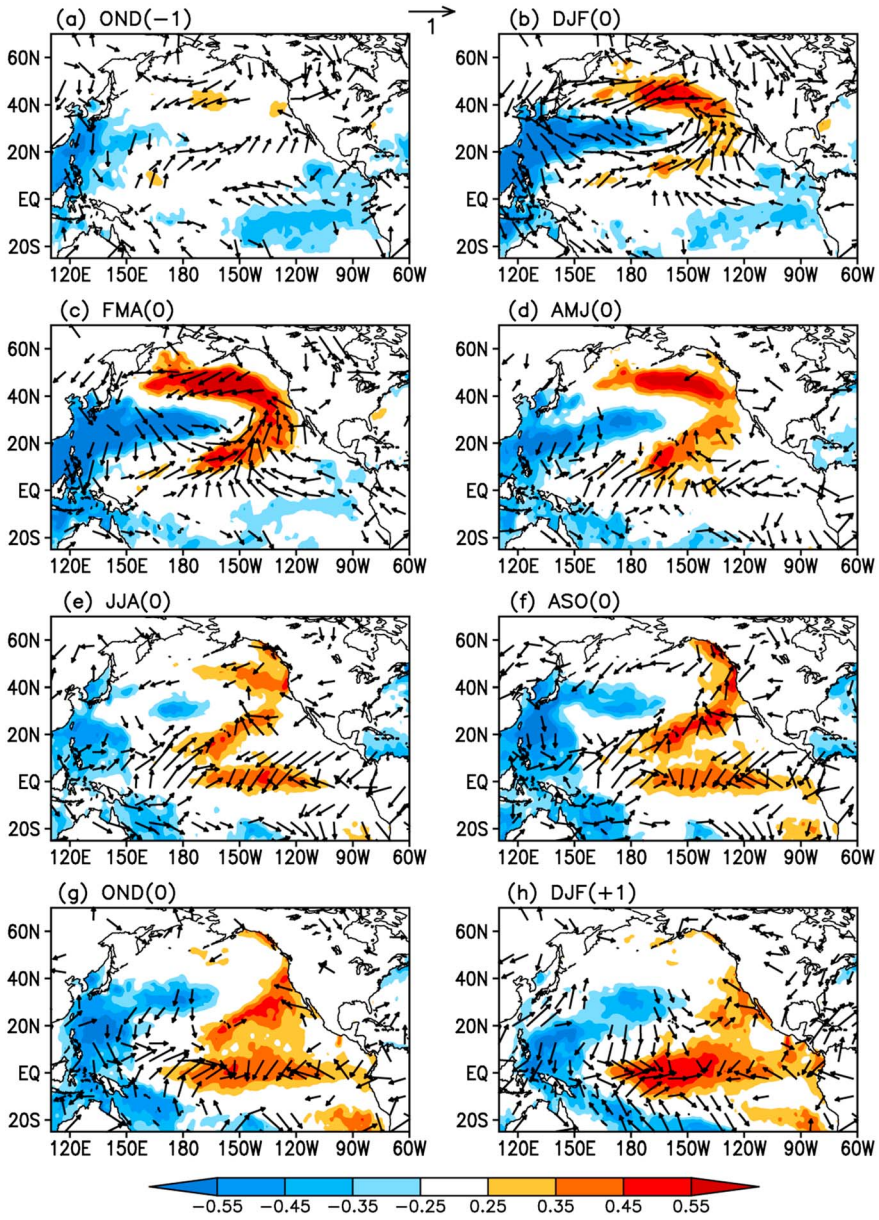

Figure 7. Correlation maps of the FMA(0)-averaged VMI with the 3 month averaged SST (shaded) and surface wind (vectors) anomalies for OND(−1), DJF(0), FMA(0), AMJ(0), JJA(0), ASO(0), OND(0), and DJF(+1). Positive (red) and negative (blue) SSTAs, with correlation significant at the 95% level, are shaded. Only surface wind vectors significant at the 95% level are shown.

4.2. Mechanisms Linking the VM to ENSO

The above results have shown a significant lead-lag relationship between variability in the VM and ENSO. But how does the VM affect ENSO? Next, we examine in detail the evolutionary features of SST, surface wind, and subsurface ocean temperature anomalies associated with the VM, with the aim of identifying possible mechanisms that contribute to the link between the VM and ENSO.

We first examine the spatial patterns of the 3 month averaged SST and surface wind anomalies correlated with the FMA(0)-averaged VMI for a range of lead-lag times (Figure 7). During October–December (OND)(−1), about 4 months before the VM peaks, significant negative SSTAs can be clearly seen in the western North Pacific (WNP) (Figure 7a). At the same time an anomalous circulation resembling the NPO develops, consistent with changes in surface wind anomalies. These results suggest that anomalous SSTAs in the WNP possibly play an important role in developing the NPO (mainly the southern pole of the NPO). Our results are also generally consistent

Table 1. Classification of Years in Which Positive or Negative VM Events Were or Were Not Followed by an El Niño or La Niña Event During the Period 1950–2011

	El Niño	No Event	La Niña
Positive VM	1957, 1965, 1968, 1982, 1986, 1991, 1997	1963, 1996	
Negative VM		1953, 1961, 1969, 2001	1988, 1998, 2000, 2007, 2008, 2010

withthe findings of T. C. D. L. Tseng et al. (The modulation of the Western North Pacific on ENSO through the Kuroshio pathway, submitted to *Climate Dynamics*, 2014), who report that the ocean-atmosphere variability in the WNP may act as a pivotal driver modulating the NPO/VM patterns through the Kuroshio pathway.

The strengthened NPO can then force a dipole-like SSTA pattern in the North Pacific north of 20°N and a subtropical positive SSTA band lying between 5°N and 20°N. During DJF(0), about 2 months before the VM peaks, a meridional tripole-like SSTA pattern can be clearly seen in the North Pacific north of 5°N (Figure 7b). As expected, this tripole-like SSTA pattern reaches a peak during FMA(0) (Figure 7c). At this time the SSTA pattern associated with the VM in the tropical central eastern Pacific closely resembles a PMM pattern [*Chiang and Vimont*, 2004; *Chang et al.*, 2007], with positive SSTAs in the subtropical central eastern North Pacific (10°N–30°N) and negative SSTAs in the tropical eastern Pacific. Note that in addition to the PMM pattern, there are significant negative SSTAs associated with the VM in the WNP. Previous studies have shown their respective importance of the PMM [*Zhang et al.,* 2009a, 2009b] and WNP [*Wang et al.*, 2012, 2013] SSTA patterns in initiating ENSO events. Given that both the PMM and WNP patterns are strongly related to the NPO [*Chiang and Vimont*, 2004; *Chang et al.*, 2007; *Wang et al.*, 2012] and the VM is closely linked to SSTAs in the subtropical central eastern North Pacific and WNP, it is likely that they are both strongly correlated to the VM. The correlations of the monthly VMI with the monthly PMM SST index (available online at http://www.esrl.noaa.gov/psd/data/timeseries/monthly/PMM/) and the monthly WNP index (defined as the area-mean SSTA over the WNP (122°E–132°E, 18°N–28°N)) are 0.44 and −0.54, respectively, both of which are significant at the 99.9% level. These results suggest that these three North Pacific climate patterns (i.e., the VM, PMM, and WNP), which are all related to the NPO, are strongly interconnected during the development of ENSO.

As the VM peaks during FMA(0), the significant positive SSTA band in the subtropical central eastern North Pacific extends toward the central equatorial Pacific (Figure 7c). At the same time, anomalous surface wind associated with the VM also extend across the entire equatorial Pacific. Anomalous southeasterlies occur in the tropical eastern Pacific, while anomalous southwesterlies occur in the tropical western Pacific, causing convergence in the central equatorial Pacific and in turn favoring the development of positive SSTAs there. During AMJ(0), significant positive SSTAs begin to establish in the central equatorial Pacific (Figure 7d). At this time, significant positive and negative SSTAs still persist in the subtropical central eastern North Pacific and WNP, respectively. The positive SSTAs in the subtropical central eastern North Pacific and central equatorial Pacific, combined with negative SSTAs in the WNP, lead to an increase in the zonal SSTA gradient across the western central tropical Pacific, which then strengthens the anomalous westerlies over the western central equatorial Pacific. After JJA(0), air-sea interaction through a positive feedback process in turn amplifies the zonal wind and SST anomalies along the equator [*Bjerknes*, 1969], driving continued growth of these anomalies. During DJF(+1), about 10 months after the VM peaks, a warming pattern is well developed in the central eastern equatorial Pacific (Figure 7h).

To further elucidate the effects of the VM-related SSTAs on the tropical Pacific overlying atmosphere during FMA(0), we performed numerical experiments with CAM5 by imposing the VM-related SSTAs in the tropical Pacific region (110°E–90°W, 10°S–35°N). The positive (or negative) VM events-related SSTAs are obtained from the composites of the FMA(0)-averaged SSTAs for positive (or negative) VM events. One positive (or negative) VM event is defined as a year when the VM index shown in Figure 6c is greater than one standard deviation (SD) or less than one negative SD (Table 1). The composite differences of the FMA(0) SSTAs between positive and negative VM events in the tropical Pacific region are shown in Figure 8a. In the control experiment (E1), CAM5 is forced with the FMA-averaged climatological SST.

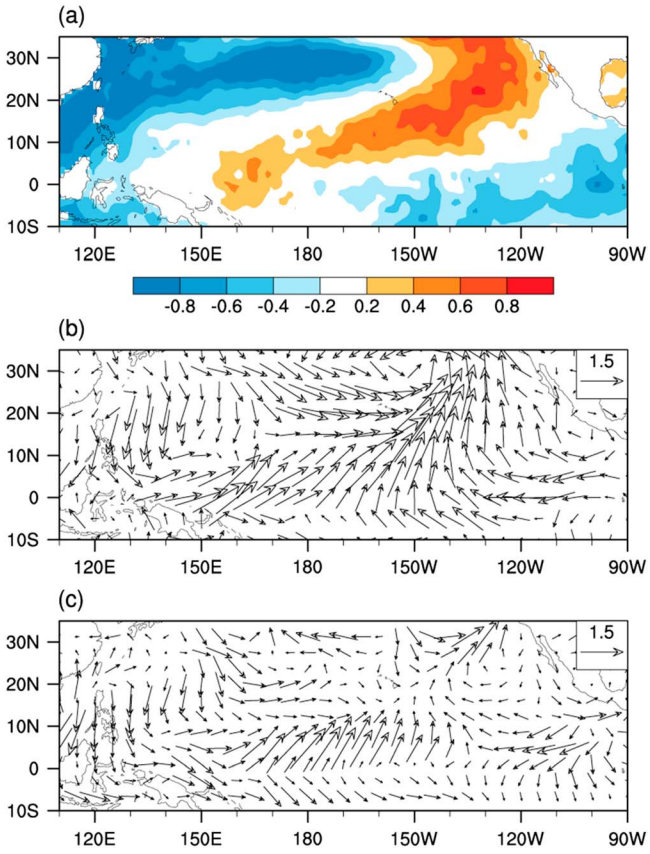

Figure 8. (a) Composite differences of the observed FMA(0) SSTAs between positive and negative VM events in the tropical Pacific region (110°E–90°W, 10°S–35°N). (b) Composite differences of the observed FMA (0) surface wind anomalies between positive and negative VM events. (c) As in (b) but for differences between numerical experiments E2 and E3 performed using the CAM5 atmospheric model.

In the positive VM-forced experiment (E2), CAM5 is forced by the FMA(0) SSTA composites for positive VM events imposed on the climatological SST only in the tropical Pacific region (110°E–90°W, 10°S–35°N). Outside this domain, the climatological SST is prescribed. The negative VM-forced experiment (E3) is same as E2, but the model is forced by the FMA(0) SSTA composites for negative VM events. The three experiments were all run for 13 years, with the first 3 years excluded for the model spin-up, and the remaining 10 years were used in the analysis.

Figure 8b shows the composite differences of the observed FMA(0) surface wind anomalies between positive and negative VM events. For comparison, Figure 8c shows the results of the model simulations. In the observations, positive VM events are associated with low-level cyclonic anomalies in the western central subtropical North Pacific and anticyclonic anomalies in the central eastern subtropical North Pacific. Consistent with these cyclonic and anticyclonic anomalies, the anomalous westerlies occur in the western central equatorial Pacific, while the anomalous easterlies occur in the eastern equatorial Pacific. Under the VM-related SSTA forcing, the simulated response of surface wind anomalies effectively captures the large-scale pattern of observed surface wind anomalies in the tropical Pacific, although the simulated surface wind anomalies are somewhat weaker than those in the observations over the tropical Pacific. Despite the crudeness of this numerical simulation, as it lacks any North Pacific extratropical forcing and air-sea feedback, the general similarity with observations leads support to the idea that VM-related SSTAs can force the tropical Pacific overlying atmosphere and in turn trigger the onset of ENSO events.

The process described above involves air-sea coupling associated with the VM in the tropical/extratropical Pacific, resembling the so-called SFM. However, note that anomalous surface winds associated with the VM extend across the entire equatorial Pacific in late winter and early spring (FMA(0), see Figure 7c), which subsequently play an important role in triggering the warming in the central equatorial Pacific. However, according to the SFM, significant SSTAs induced by the NPO persist until late spring and summer when they subsequently influence the equatorial wind fields and hence the underlying SSTs [*Vimont et al.*, 2001, 2003a, 2003b]. Therefore, we conclude that the mechanism through which the VM affects ENSO is slightly different from the SFM (similar to the SFM but a different lag response of the equatorial wind and SST anomalies to the North Pacific extratropical forcing). A possible explanation for this difference may be that SST and surface wind anomalies associated with the VM extend much farther toward the equator than those associated with the NPO (not shown). Consequently, the SST and surface wind responses in the equatorial Pacific to the VM are stronger and more immediate. At this point, the VM is similar to the PMM, which also peaks in late winter and spring and affects the SST and surface winds in the tropical Pacific immediately at its peak phase [*Chiang and Vimont*, 2004; *Chang et al.*, 2007]. However, as mentioned above,

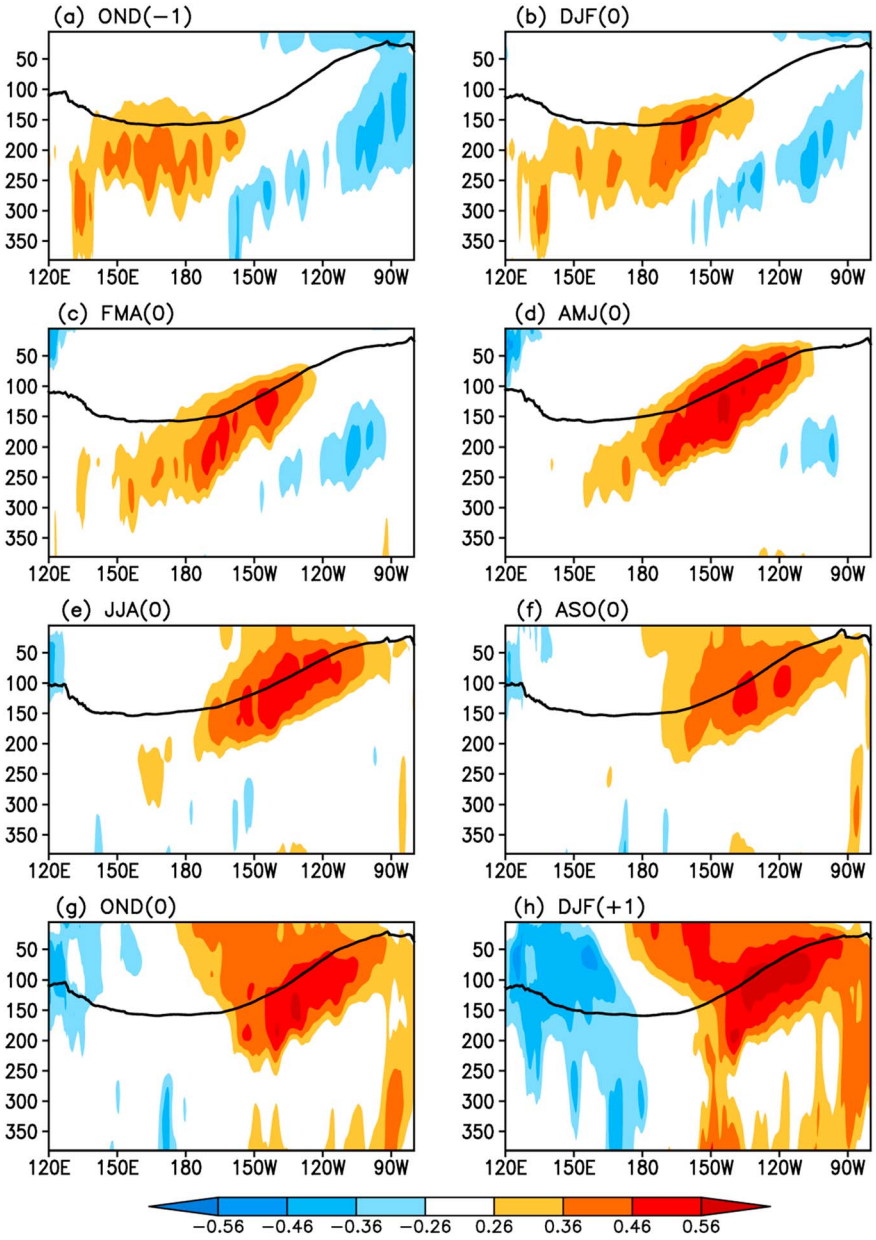

Figure 9. Correlation maps of the FMA(0)-averaged VMI with the 3 month averaged subsurface ocean temperature anomalies at different depths in meters averaged over 5°S–5°N for OND(−1), DJF(0), FMA(0), AMJ(0), JJA(0), ASO(0), OND(0), and DJF(+1). Areas with correlation significant at the 95% level are shaded. Thick black contour indicates the climatological position of the 23°C isotherm.

the VM, as a basin-scale North Pacific SST pattern, combines the active role of SSTAs in both the central eastern North Pacific and the WNP, different from the PMM pattern that mainly emphasizes the critical role of SSTAs in the central eastern North Pacific as a precursor to ENSO but considers less the independent contribution of SSTAs in the WNP to the initiation of ENSO events. In other words, the VM may play a unique role (i.e., as a basin-scale influence as opposed to the more local influence of the PMM or SFM) in forcing subsequent ENSO events.

In addition to significant SST and surface wind anomalies in the equatorial Pacific, subsurface temperature anomalies across the equatorial Pacific are found to be closely related to the VM. Figure 9 shows correlation maps of the FMA(0)-averaged VMI with the 3 month averaged subsurface temperature anomalies at different

depths averaged over 5°S–5°N for a range of lead-lag times. During OND(–1), significant positive subsurface temperature anomalies form in the western central equatorial Pacific (between 130°E and 150°W) at around 100–300 m depth (Figure 9a). These positive subsurface temperature anomalies are likely from La Niña events which tend to occur prior to El Niño events due to the biennial oscillation embedded in ENSO variability. They are also likely generated by the same NPO-related surface wind anomalies that induce the VM [*Anderson*, 2004; *Anderson et al.*, 2013a]. It seems unlikely that the VM plays an active role in generating these subsurface temperature anomalies, considering that significant subsurface temperature anomalies occur during OND(–1), prior to the peak of the VM during FMA(0).

Afterward these positive subsurface temperature anomalies propagate eastward and upward along the thermocline (Figures 9b–9e), reaching the eastern equatorial Pacific during JJA(0), when they start to warm the surface waters. In this case, there is significant warming over the central eastern equatorial Pacific (between 150°W and 120°W), despite the fact that in the eastern equatorial Pacific anomalous easterlies tend to enhance upwelling and cool the surface. We speculate that surface wind anomalies associated with the VM may play an important role in the evolution of subsurface ocean temperature anomalies once these subsurface temperature anomalies are generated. *Anderson et al.* [2013a] argued that the mechanism responsible for such evolution of subsurface ocean temperature anomalies is fundamentally different from the SFM, which does not influence the structure of the subsurface equatorial Pacific until the following late spring and summer [*Vimont et al.,* 2001, 2003a, 2003b]. They hypothesized that the equatorial Pacific subsurface temperature anomalies are a response to SLP-generated variations in the North Pacific trade winds, which they term the TWC mechanism of the equatorial Pacific.

The above analyses suggest that the onset of ENSO in response to the NPO/VM involve the following two main processes: (1) surface air-sea coupling associated with the VM in the subtropical/tropical Pacific, which generates the initial warming in the central eastern equatorial Pacific during late spring and early summer and (2) evolution of subsurface ocean temperature anomalies along the equator associated with the VM, which reinforces the warming in the central eastern equatorial Pacific during summer. As mentioned above, these two processes have been explained by several different mechanisms in previous studies [*Vimont et al.,* 2001, 2003a, 2003b; *Anderson*, 2004; *Chiang and Vimont*, 2004; *Chang et al.*, 2007; *Anderson et al.*, 2013a], which mainly emphasized extratropical influence on ENSO. We emphasize that our results here do not exclude the effects of tropical preconditioning on ENSO. Note that in Figure 7 significant negative SSTAs occur in the WNP and eastern tropical Pacific during OND(–1). On the one hand, these persistent SSTAs over the WNP and eastern tropical Pacific possibly play an important role in developing the NPO and hence VM [*Yu and Kim*, 2011; T. C. D. L. Tseng et al., submitted manuscript, 2014]; on the other hand, these SSTAs along with anomalous surface winds possibly also exert influences on the tropics [*Wang et al.*, 2012, 2013]. As the VM peaks during FMA(0), SST and surface wind anomalies associated with the VM extend across the equator, tending to strengthen the surface temperature and wind anomalies induced by the tropical preconditioning. This mechanism involving tropical-extratropical interaction may contribute to the onset of a particular ENSO event. Further study is necessary to test the robustness of such a tropical-extratropical interaction in the link between the NPO/VM and ENSO.

4.3. Classification of VM Events According to Their Link With ENSO

We next take a close examination of the two MCA time series in Figure 6c. It is noted that not every positive or negative VM event is followed by El Niño or La Niña event (same as the definition of a VM event). The question naturally arises as to why some VM events can excite ENSO while some cannot. To address this question, we classify all of the VM events according to their link with ENSO into the following two groups: (1) positive (negative) VM events that are followed by an El Niño (La Niña) event (hereafter positive VM-El Niño or negative VM-La Niña) and (2) positive (negative) VM events that are not followed by an ENSO event (hereafter positive VM only or negative VM only) (Table 1). Note that roughly 70% of the VM events (14 out of 20 events) fall into the first group.

Figure 10 shows composite differences of the 3 month averaged SST and surface wind anomalies between positive VM-El Niño and negative VM-La Niña (left panel), and between positive VM only and negative VM only (right panel) for FMA(0), AMJ(0), JJA(0), August–October (ASO)(0), and OND(0). SST and surface wind anomalies in VM-ENSO and VM only are almost identical in the North Pacific poleward of 20°N, and the major difference between both groups mainly lies in the tropics. For VM-ENSO, significant SST and surface wind

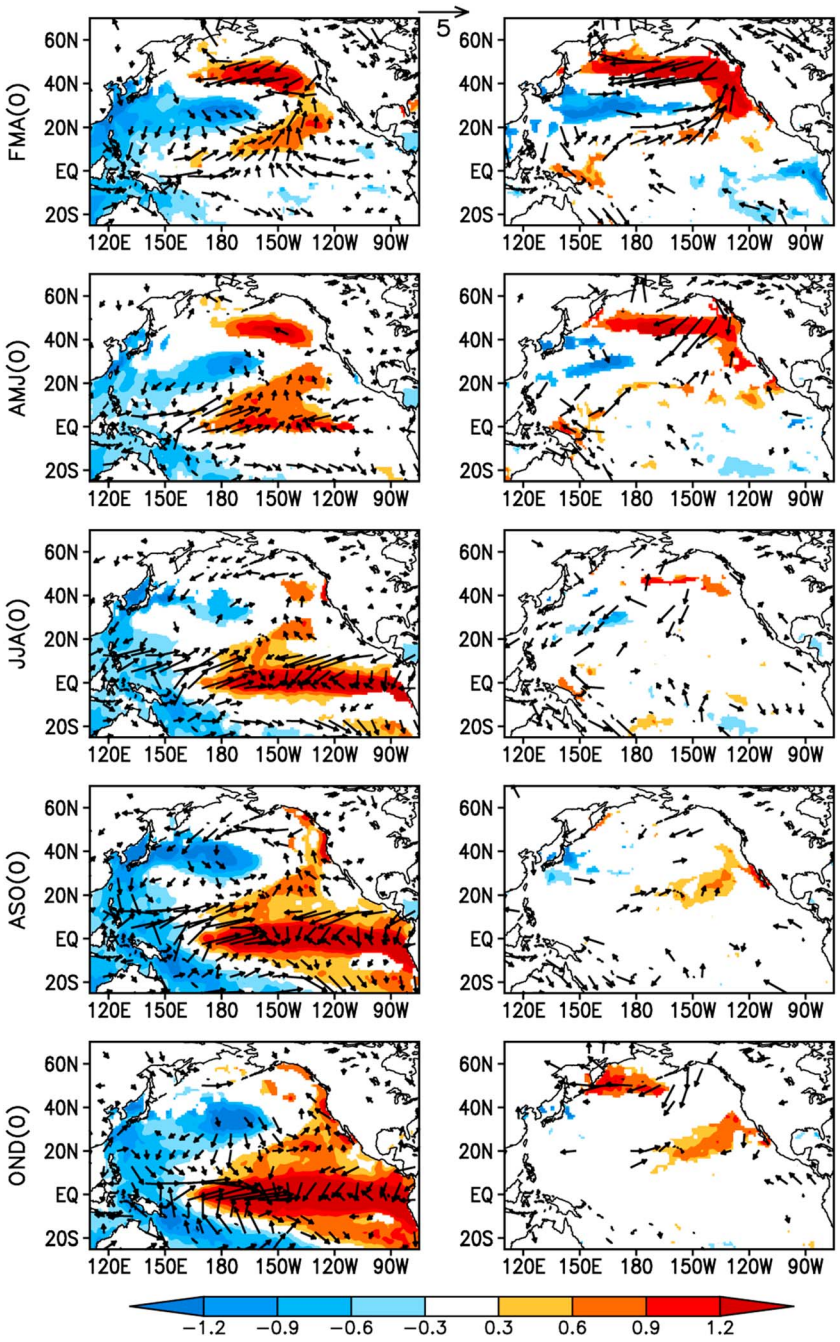

Figure 10. Composite differences of the 3 month averaged SST (shaded) and surface wind (vectors) anomalies (left) between positive VM-El Niño and negative VM-La Niña and (right) between positive VM only and negative VM only for FMA(0), AMJ(0), JJA(0), ASO(0), and OND(0) (top to bottom). Only SSTAs and surface wind vectors significant at the 90% level are shown.

anomalies associated with the VM extend farther across the equator, and by AMJ(0) the warming has established in the equatorial Pacific, with maximum warming in the central eastern equatorial Pacific. In contrast, for VM only, SST and surface wind anomalies associated with the VM have large amplitudes mainly confined north of around 20°N and do not extend sufficiently into the equator. As a result, both processes of surface air-sea coupling and subsurface ocean temperature evolution (not shown) along the equator are weak in VM only, and the warming in the central eastern equatorial Pacific does not start until JJA(0). These

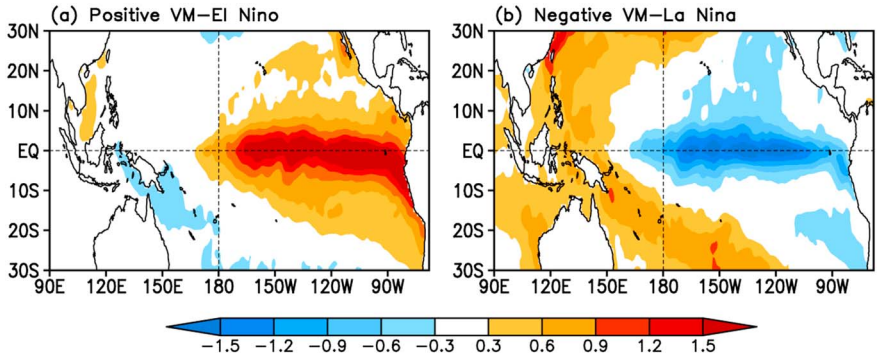

Figure 11. Composites of the JFM(+1) averaged SSTAs for (a) positive VM-El Niño and (b) negative VM-La Niña events, as listed in Table 1.

results suggest that although the VM events have a similar condition in the North Pacific poleward of 20°N (the domain over which the VM is defined), the condition alone does not ensure the development of an ENSO event. Therefore, in order to better judge whether or not a VM event is followed by an ENSO event, it is also important to consider the subtropical/tropical conditions associated with the VM. If SST and surface wind anomalies associated with the VM extend sufficiently into the equator during the late winter and early spring, it is very likely that the VM can induce an ENSO event in the following winter. Consistent with surface wind anomalies, significant SLP anomalies associated with the VM also extend less far toward the equator in VM-ENSO than in VM only (not shown). This finding is generally consistent with the view that ENSO is correlated most closely with the southern pole of the NPO, not so much with the northern one [*Anderson*, 2003].

In addition, it is important to point out that some ENSO events (8 out of 22 events according to Figure 6c) are not preceded by VM events (hereafter ENSO only). Considering that the VM works as an ocean bridge (or conduit) for the extratropical influence on ENSO, it is very likely that some tropical phenomena, such as the Madden-Julian oscillation (MJO) [*Madden and Julian*, 1994] and westerly wind bursts (WWBs) [*McPhaden et al.*, 1992; *McPhaden*, 1999], play an important role in triggering the onset of El Niño or La Niña events in ENSO only. The study of the tropical effects on the onset of ENSO in ENSO only is beyond the scope of the present paper but is a worthy topic for future research.

4.4. Relationships of the VM With Two Types of ENSO

As described above, the warming center during the peak phase of ENSO related to the VM is mostly located in the central equatorial Pacific, covering the Niño3.4 region and eastern part of the Niño4 region (see Figure 5b). The peak correlation between the VM and Niño4 (and also EM) indices is higher than that between the VM and Niño3 indices (Figure 5a). Although the warming center related to the VM is located in the central equatorial Pacific, the eastern equatorial Pacific SST is dominated by positive (not negative) anomalies, as also seen in Figure 6b. *Ashok et al.* [2007] reported that a typical EM pattern shows positive SSTAs in the central tropical Pacific but negative SSTAs in the western and eastern tropical Pacific. This indicates that the VM is followed not merely by a typical EM pattern and seems to be followed by a mixed pattern of EM and conventional El Niño. The fact that several positive VM events are followed by EM events (such as 1986/1987 and 1991/1992) [*Ashok et al.*, 2007] but other several positive VM events are followed by conventional El Niño events (such as 1982/1983 and 1997/1998) supports this speculation (Table 1). It should be noted that the classification of two types of El Niño events remains controversial because their definitions are diverse [e.g., *Larkin and Harrison*, 2005; *Ashok et al.*, 2007; *Kao and Yu*, 2009; *Kug et al.*, 2009]. For instance, the 1986/1987 El Niño event is also classified as a conventional El Niño event [*Yu et al.*, 2012]. Nevertheless, the results in the following analysis do not change whether or not the 1986/1987 El Niño event is classified as a conventional El Niño or EM event.

In addition, it has been noted that La Niña events usually shift to the west compared to El Niño events [*Kug et al.*, 2009]. Furthermore, *Anderson et al.* [2013b] reported that the structure of ENSO events can be modulated by the sign of the precursor SLP (and presumably VM) patterns, and the preceding SLP index-related El Niño (or La Niña) events tend to shift more eastward (or westward). Figures 11a and 11b

shows the composites of the JFM(+1) averaged SSTAs for positive VM-El Niño and negative VM-La Niña events (as listed in Table 1), respectively. We can see that VM-induced La Niña events are located more westward (i.e., centrally) than VM-induced El Niño events, consistent with the findings of *Anderson et al.* [2013b]. The positioning of the VM-induced ENSO events is sign dependent, which may also result in the mixed pattern of SSTAs related to the VM.

The above analyses indicate that the VM can induce EM as well as conventional El Niño. We find that there is no clear difference between the precursor VM patterns of two types of El Niño events by analyzing the composites of the 3 month averaged SSTAs for two EM events (1986/1987 and 1991/1992) and two conventional El Niño events (1982/1983 and 1997/1998) preceded by the VM events (not shown). It is speculated that while the VM may trigger the initial warming in the equatorial Pacific, we do not exclude other possible mechanisms involving tropical coupled dynamics that act to further develop the initial warming in the tropical Pacific, having been triggered by the VM, respectively, to the EM and conventional El Niño patterns. Given the limited number of available events in observations, further study is required using a coupling ocean-atmosphere general circulation model to further examine the differences between the precursor signals of two types of El Niño events.

5. Summary and Discussion

This study investigated the VM, which is defined as the EOF2 of SSTAs in the North Pacific (124.5°E–100.5°W, 20.5°N–65.5°N), and its link to tropical SST variability. The VM is forced by the atmosphere via the NPO, and a large fraction (>60%) of the VM variability can be explained by the NPO atmospheric forcing. The VM variations are closely linked to ENSO. The peak correlations (significant at the 99.9% level) between the VM and various ENSO indices (including the Niño3, Niño3.4, and Niño4 indices) occur when the VM leads ENSO by around 11 months, indicating that the VM may be a precursor for ENSO events. Furthermore, the VM tends to peak in late winter and early spring, right before the spring predictability barrier (SPB) of ENSO [*Webster and Yang*, 1992]. We speculate that, if strong VM events could be successfully predicted and the VM-ENSO precursor relationship could be well captured by the forecast models, this may enhance our confidence in those ENSO forecasts that are preceded by a VM event.

Our results are consistent with many previous studies that have identified the NPO or SLP anomalies in the subtropical North Pacific as the precursor signature for ENSO events [e.g., *Vimont et al.,* 2001, 2003a, 2003b; *Anderson*, 2003]. However, our results emphasize that the VM, as an ocean bridge connecting the NPO and ENSO, is more directly linked to ENSO than is the NPO. The fact that the VM has stronger and more significant correlations with ENSO than the NPO for lead times of a few months to more than a year supports our findings. The present analyses suggest that the VM can trigger the onset of ENSO via the following two dominant processes: (1) surface air-sea coupling associated with the VM in the subtropical/tropical Pacific and (2) evolution of subsurface ocean temperature anomalies along the equator associated with the VM. The former affects the SST and surface winds in the tropical Pacific immediately after the peak of the VM and generates the initial warming in the central eastern equatorial Pacific during late spring and early summer. The latter may cause the subsurface ocean temperature anomalies along the equator to propagate eastward and upward and to reach the surface during summer, reinforcing the warming in the central eastern equatorial Pacific. Finally, these two processes may produce sufficient surface warming in the central eastern equatorial Pacific, causing an ENSO event to develop.

The strong correlation between the VM and ENSO about a year later highlights the potential importance of the VM in contributing to ENSO development. However, note that not every VM event is followed by an ENSO event. We found that over the period 1950–2011, roughly 30% of the VM events (6 out of 20 events) did not lead to an ENSO event. SST and surface wind anomalies associated with these VM events seem to extend less far toward the equator than those associated with other VM events. As a result, both processes of surface air-sea coupling and subsurface ocean temperature evolution are weak in the equatorial Pacific, making these VM events ineffective in generating warming in the central eastern equatorial Pacific. In addition, the VM can induce EM as well as conventional El Niño. There is no evidence that the VM tends to be more conducive to the initialization of EM than conventional El Niño.

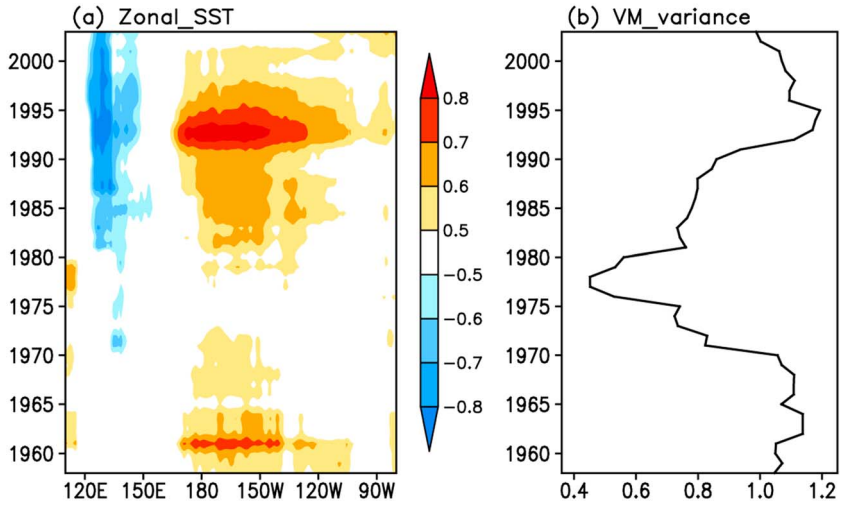

Figure 12. (a) The 15 year moving correlations between the FMA(0) VMI and JFM(+1) SSTAs averaged over 5°S–5°N for the period 1950–2011. Areas with correlation significant at the 95% level are shaded. (b) Time series of running SD of the FMA (0) VMI calculated within a 15 year window that moves year by year for the period 1950–2011.

Recent studies have noted that the VM-related SST variability in the North Pacific becomes more pronounced in the 1990s [*Bond et al.*, 2003; *Yu et al.*, 2010]. Figure 12b shows that the interannual variability of the VM exhibits a marked decadal change, with the highest SD in the 1990s and the lowest SD in the 1970s, generally consistent with the findings of *Bond et al.* [2003] and *Yu et al.* [2010]. Decadal variations of the VM are generally consistent with its relationship with ENSO. Note that a stronger VM corresponds with a strengthened relationship between the VM and SSTAs in the equator in the 1990s; in contrast, a weaker VM corresponds with a weakened relationship between the VM and SSTAs in the equator in the 1970s (Figure 12a). These results suggest that a stronger VM tends to exert a stronger influence on the tropics. However, the physical mechanisms responsible for decadal changes in the VM remain unexplained. Several recent studies have suggested that the NPO and hence VM-related SST variability in the North Pacific possibly arise from tropical SST forcing [*Di Lorenzo et al.*, 2010; *Yu and Kim*, 2011; T. C. D. L. Tseng et al., submitted manuscript, 2014]. It is unclear whether the strengthening VM in recent decades is linked to tropical forcing or to global warming. Further study is necessary to examine the underlying mechanisms responsible for decadal changes in the VM.

Acknowledgments
We wish to thank three anonymous reviewers for helpful comments and suggestions. This research was jointly supported by the 973 project of China (2012CB955200), the Strategic Priority Research Program of the Chinese Academy of Sciences (XDA11010303), and the National Natural Science Foundation of China (41175069). The SODA data set was obtained from the National Center for Atmospheric Research (NCAR). The atmospheric reanalysis data set was obtained from the National Centers for Environmental Prediction-National Center for Atmospheric Research (NCEP-NCAR). The HadISST data set was obtained from the Met Office Hadley Centre. The EM index was made available online at www.jamstec.go.jp/frsgc/research/d1/iod/DATA/emi.monthly.txt. The NPGO index was made available online at http://www.o3d.org/npgo/data/NPGO.txt. The PMM SST index was made available online at http://www.esrl.noaa.gov/psd/data/timeseries/monthly/PMM/.

References

Alexander, M. A., D. J. Vimont, P. Chang, and J. D. Scott (2010), The impact of extratropical atmospheric variability on ENSO: Testing the seasonal footprinting mechanism using coupled model experiments, *J. Clim.*, *23*, 2885–2901.
Anderson, B. T. (2003), Tropical Pacific sea-surface temperatures and preceding sea level pressure anomalies in the subtropical North Pacific, *J. Geophys. Res.*, *108*(D23), 4732, doi:10.1029/2003JD003805.
Anderson, B. T. (2004), Investigation of a large-scale mode of ocean–atmosphere variability and its relation to tropical Pacific sea surface temperature anomalies, *J. Clim.*, *17*, 4089–4098.
Anderson, B. T., R. C. Perez, and A. Karspeck (2013a), Triggering of El Niño onset through trade wind-induced charging of the equatorial Pacific, *Geophys. Res. Lett.*, *40*, 1212–1216, doi:10.1002/grl.50200.
Anderson, B. T., J. C. Furtado, K. M. Cobb, and E. Di Lorenzo (2013b), Extratropical forcing of El Niño–Southern Oscillation asymmetry, *Geophys. Res. Lett.*, *40*, 4916–4921, doi:10.1002/grl.50951.
Ashok, K., S. K. Behera, S. A. Rao, H. Weng, and T. Yamagata (2007), El Niño Modoki and its possible teleconnection, *J. Geophys. Res.*, *112*, C11007, doi:10.1029/2006JC003798.
Bjerknes, J. (1969), Atmospheric teleconnections from the equatorial Pacific, *Mon. Weather Rev.*, *97*, 163–172.
Bond, N. A., J. E. Overland, M. Spillane, and P. Stabeno (2003), Recent shifts in the state of the North Pacific, *Geophys. Res. Lett.*, *30*(23), 2183, doi:10.1029/2003GL018597.
Bretherton, C. S., C. Smith, and J. M. Wallace (1992), An intercomparison of methods for finding coupled patterns in climate data, *J. Clim.*, *5*, 541–560.
Bretherton, C. S., M. Widmann, V. P. Dymnidov, J. M. Wallace, and I. Blade (1999), The effective number of spatial degrees of freedom of a time-varying field, *J. Clim.*, *12*, 1990–2009.
Carton, J. A., and B. S. Giese (2008), A reanalysis of ocean climate using Simple Ocean Data Assimilation (SODA), *Mon. Weather Rev.*, *136*, 2999–3017.
Ceballos, L. I., E. Di Lorenzo, C. D. Hoyos, N. Schneider, and B. Taguchi (2009), North Pacific gyre oscillation synchronizes climate fluctuations in the eastern and western boundary systems, *J. Clim.*, *22*, 5163–5174.

Chang, P., L. Zhang, R. Saravanan, D. J. Vimont, J. C. H. Chiang, L. Ji, H. Seidel, and M. K. Tippett (2007), Pacific meridional mode and El Niño–Southern Oscillation, *Geophys. Res. Lett.*, *34*, L16608, doi:10.1029/2007GL030302.

Chhak, K., E. Di Lorenzo, N. Schneider, and P. F. Cummins (2009), Forcing of low-frequency ocean variability in the Northeast Pacific, *J. Clim.*, *22*, 1255–1276.

Chiang, J., and D. Vimont (2004), Analogous Pacific and Atlantic meridional modes of tropical atmosphere-ocean variability, *J. Clim.*, *17*, 4143–4158.

Deser, C., and A. S. Phillips (2006), Simulation of the 1976/1977 climate transition over the North Pacific: Sensitivity to tropical forcing, *J. Clim.*, *19*, 6170–6180.

Deser, C., M. A. Alexander, and M. S. Timlin (2003), Understanding the persistence of sea surface temperature anomalies in midlatitudes, *J. Clim.*, *16*, 57−72.

Di Lorenzo, E., et al. (2008), North Pacific Gyre Oscillation links ocean climate and ecosystem change, *Geophys. Res. Lett.*, *35*, L08607, doi:10.1029/2007GL032838.

Di Lorenzo E., et al. (2009a), Nutrient and salinity decadal variations in the central and eastern North Pacific, *Geophys. Res. Lett.*, *36*, L14601, doi:10.1029/2009GL038261.

Di Lorenzo E., N. Schneider, K. M. Cobb, J. Furtado, and M. Alexander (2009b), ENSO and the North PacificGyre Oscillation: An integrated view of Pacificdecadal dynamics, a talk given at a 2-day workshop on 'Exploring the predictability and mechanisms of Pacific low frequency variability beyond inter-annual time scales', held on October 24–25 at the 2009 PICES Annual Meeting in Jeju, Korea.

Di Lorenzo, E., K. M. Cobb, J. C. Furtado, N. Schneider, B. T. Anderson, A. Bracco, M. A. Alexander, and D. J. Vimont (2010), Central Pacific El Niño and decadal climate change in the North Pacific Ocean, *Nat. Geosci.*, *3*, 762–765.

Ding, R. Q., and J. P. Li (2009), Decadal and seasonal dependence of North Pacific SST persistence, *J. Geophys. Res.*, *114*, D01105, doi:10.1029/2008JD010723.

Furtado, J. C., E. Di Lorenzo, B. T. Anderson, and N. Schneider (2012), Linkages between the North Pacific Oscillation and central tropical Pacific SSTs at low frequencies, *Clim. Dyn.*, *39*, 2833–2846.

Graham, N. (1994), Decadal scale variability in the 1970's and 1980's: Observations and model results, *Clim. Dyn.*, *10*, 60–70.

Hare, S. R., and N. J. Mantua (2000), Empirical evidence for North Pacific regime shifts in 1977 and 1989, *Prog. Oceanogr.*, *47*, 103–146.

Kalnay, E., et al. (1996), The NCEP–NCAR 40-year reanalysis project, *Bull. Am. Meteorol. Soc.*, *77*, 437–471.

Kao, H.-Y., and J.-Y. Yu (2009), Contrasting eastern Pacific and central Pacific types of ENSO, *J. Clim.*, *22*, 615–632.

Kug, J.-S., F.-F. Jin, and S.-I. An (2009), Two types of El Niño events: Cold tongue El Niño and warm pool El Niño, *J. Clim.*, *22*, 1499–1515.

Larkin, N. K., and D. E. Harrison (2005), Global seasonal temperature and precipitation anomalies during El Niño autumn and winter, *Geophys. Res. Lett.*, *32*, L16705, doi:10.1029/2005GL022860.

Madden, R. A., and P. R. Julian (1994), Observations of the 40–50-day tropical oscillation—A review, *Mon. Weather Rev.*, *122*, 814−837.

Mantua, N. J., and S. R. Hare (2002), The Pacific decadal oscillation, *J. Oceanogr.*, *58*, 35–44.

Mantua, N. J., S. R. Hare, Y. Zhang, J. M. Wallace, and R. C. Francis (1997), A Pacific interdecadal climate oscillation with impacts on salmon production, *Bull. Am. Meteorol. Soc.*, *78*, 1069–1079.

McPhaden, M. J. (1999), Genesis and evolution of the 1997–98 El Niño, *Science*, *283*, 950–954.

McPhaden, M. J., F. Bahr, Y. D. Penhoat, E. Firing, S. P. Hayes, P. P. Niiler, P. L. Richardson, and J. M. Toole (1992), The response of the western equatorial Pacific Ocean to westerly wind bursts during November 1989 to January 1990, *J. Geophys. Res.*, *97*, 14,289–14,303, doi:10.1029/92JC01197.

Miller, A. J., D. R. Cayan, T. P. Barnett, N. E. Graham, and J. M. Oberhuber (1994), The 1976–77 climate shift of the Pacific Ocean, *Oceanography*, *7*, 21–26.

Neale, R. B., et al. (2010), Description of the NCAR Community Atmosphere Model (CAM5), *Tech. Rep. NCAR/TN-486+STR*, 268 pp., Natl. Cent. for Atmos. Res., Boulder, Colo.

Newman, M., G. P. Compo, and M. A. Alexander (2003), ENSO-forced variability of the Pacific decadal oscillation, *J. Clim.*, *16*, 3853–3857.

Nitta, T., and S. Yamada (1989), Recent warming of tropical sea surface temperature and its relationship to the Northern Hemisphere circulation, *J. Meteorol. Soc. Jpn.*, *67*, 375–383.

Penland, C., and P. D. Sardeshmukh (1995), The optimal growth of tropical sea surface temperature anomalies, *J. Clim.*, *8*, 1999–2024.

Rayner, N. A., P. Brohan, D. E. Parker, C. K. Folland, J. J. Kennedy, M. Vanicek, T. Ansell, and S. F. B. Tett (2006), Improved analyses of changes and uncertainties in sea surface temperature measured in situ since the mid-nineteenth century: The HadSST2 dataset, *J. Clim.*, *19*, 446–469.

Rogers, J. C. (1981), The North Pacific Oscillation, *J. Climatol.*, *1*, 39–57.

Schneider, N., and B. Cornuelle (2005), The forcing of the Pacific decadal oscillation, *J. Clim.*, *18*, 4355–4373.

Trenberth, K., and J. Hurrell (1994), Recent observed interdecadal climate changes in the Northern Hemisphere, *Clim. Dyn.*, *9*, 303–319.

Tzeng, W.-N., Y.-H. Tseng, Y.-S. Han, C.-C. Hsu, C.-W. Chang, E. Di Lorenzo, and C.-H. Hsieh (2012), Evaluation of multi-scale climate effects on annual recruitment levels of the Japanese eel, Anguilla japonica, to Taiwan, *PLoS One*, *7*, doi:10.1371/journal.pone.0030805.

Vimont, D. J., D. S. Battisti, and A. C. Hirst (2001), Footprinting: A seasonal connection between the tropics and mid-latitudes, *Geophys. Res. Lett.*, *28*, 3923–3926, doi:10.1029/2001GL013435.

Vimont, D. J., J. M. Wallace, and D. S. Battisti (2003a), The seasonal footprinting mechanism in the Pacific: Implications for ENSO, *J. Clim.*, *16*, 2668–2675.

Vimont, D. J., D. S. Battisti, and A. C. Hirst (2003b), The seasonal footprinting mechanism in the CSIRO general circulation models, *J. Clim.*, *16*, 2653–2667.

Walker, G. T., and E. W. Bliss (1932), World weather V, *Mem. R. Meteorol. Soc.*, *4*, 53–84.

Wang, S.-Y., M. L'Heureux, and H.-H. Chia (2012), ENSO prediction one year in advance using western North Pacific sea surface temperatures, *Geophys. Res. Lett.*, *39*, L05702, doi:10.1029/2012GL050909.

Wang, S.-Y., M. L'Heureux, and J.-H. Yoon (2013), Are greenhouse gases changing ENSO precursors in the western North Pacific, *J. Clim.*, *26*, 6309–6322.

Webster, P. J., and S. Yang (1992) Monsoon and ENSO: Selectively interactive systems, *Q. J. R. Meteorol. Soc.*, *118*, 877−925.

Yeh, S.-W., J.-S. Kug, B. Dewitte, M. H. Kwon, B. P. Kirtman, and F.-F. Jin (2009), El Niño in a changing climate, *Nature*, *461*, 511–514.

Yu, J.-Y., and S. T. Kim (2011), Relationships between extratropical sea level pressure variations and the central Pacific and eastern Pacific types of ENSO, *J. Clim.*, *24*, 708–720.

Yu, J.-Y., H.-Y. Kao, and T. Lee (2010), Subtropics-related interannual sea surface temperature variability in the central equatorial Pacific, *J. Clim.*, *23*, 2869–2884.

Yu, J.-Y., Y.-H. Zhou, S. T. Kim, T. Lee (2012), The changing impact of El Niño on US winter temperatures, *Geophys. Res. Lett.*, *39*, L05702, doi:10.1029/2012GL052483.
Zhang, L., P. Chang, and L. Ji (2009a), Linking the Pacific meridional mode to ENSO: Coupled model analysis, *J. Clim.*, *22*, 3488–3505.
Zhang, L., P. Chang, and M. K. Tippett (2009b), Linking the Pacific meridional mode to ENSO: Utilization of a noise filter, *J. Clim.*, *22*, 905–922.
Zhang, Y., J. M. Wallace, and D. S. Battisti (1997), ENSO-like interdecadal variability, *J. Clim.*, *10*, 1004–1020.